Automatic Optimization Method Based on Mesh Morphing Surface Sculpting Driven by Biological Growth Method: An Application to the Coiled Spring Section Shape

Stefano Porziani, Francesco de Crescenzo, Emanuele Lombardi, Christian Iandiorio, Pietro Salvini, Marco Evangelos Biancolini

Automatic Optimization Method Based on Mesh Morphing Surface Sculpting Driven by Biological Growth Method: An Application to the Coiled Spring Section Shape

Stefano Porziani(✉), Francesco De Crescenzo, Emanuele Lombardi, Christian Iandiorio, Pietro Salvini, and Marco Evangelos Biancolini

University of Rome "Tor Vergata", Via del Politecnico 1, 00133 Rome, Italy
porziani@ing.uniroma2.it

Abstract. The increasing importance of optimization in manufacturing processes led to the improvement of well established optimization techniques and to the development of new and innovative approaches. Among these, an approach that exploits surface stresses distribution to obtain an optimized configuration is the Biological Growth Method (BGM). Coupling this method with surface sculpting based on Radial Basis Functions (RBF) mesh morphing had proven to be efficient and effective in optimizing specific mechanical components. In this work, the automatic, meshless and constrained parameter-less optimization approach is applied to a classical mechanical component and then compared with a parameter-based shape optimisation result.

Keywords: Parameter-less optimization · Mesh morphing · Automatic surface sculpting · Coiled spring

1 Introduction

Optimization of manufactured mechanical components is an important phase of every production process. The optimal configuration achievement is a process which requires a lot of design efforts and that can be lowered adopting numerical techniques. Computer Aided Design (CAD), can support designers in every phase of the product manufacturing. Finite Element Method (FEM) gave an important speed up to design tasks, allowing designer to numerically test performances of different configurations before realising a test prototype. These activities, however, can be very time consuming: mesh morphing [3,8,22] had been introduced in the design process to obtain shape variation without the need to generate a modified geometry. Thanks to the high reliability of the Radial Basis Functions (RBF) based mesh morphing, this mesh-less technique

M. Paszynski et al. (Eds.): ICCS 2021, LNCS 12746, pp. 479–491, 2021.
https://doi.org/10.1007/978-3-030-77977-1_38

had been successfully adopted into various engineering workflows. Among the various engineering applications that had benefits in adopting mesh morphing it is possible to report Fluid Structure Interaction (FSI) [5,12,16], or crack front propagation prediction [9], as reported in [10] and [6].

Mesh morphing acts directly on the numerical model, by modifying the calculation grid nodes position without considering the underlying geometry used to generate the grid. This shape modification can also be applied using numerical results obtained with the same numerical model to be optimized, exploiting, for example, adjoint data [11,18] or using the Biological Growth Method (BGM) [20]. BGM mimics the way natural tissues, such as tree trunks and bones, evolve to mitigate stress peaks on their surfaces. The BGM has been successfully employed in mechanical component shape optimization [20], and had proven its reliability in optimization also compared with parameter-based optimization methods [19] and with other parameter-less methods [20].

In the present work, the optimization procedure [21] based on BGM and using RBF mesh morphing to automatically sculpt a mechanical component surfaces is first presented and then used to optimize a cross section of the coiled spring, comparing results with the ones achieved adopting the classical circular cross section and the ones computed with a parameter-based optimisation.

The tools adopted for the generation, optimization and analysis of the numerical model are included in the ANSYS Workbench Finite Element Analysis (FEA) framework [1]. The RBF Morph ACT extension [2] is used to apply RBF based mesh morphing driven by the BGM algorithm.

2 Recall on the Theoretical Background

In this section an overview on parameter-less optimization methodology is given, describing first the RBF based mesh morphing procedure (Sect. 2.1), then the BGM used to drive the morphing action (Sect. 2.2), and then concluding with the description of the coupling of these two techniques to obtain a surface sculpting optimization procedure (Sect. 2.3).

2.1 RBF Based Mesh Morphing

RBF was at first employed as a mathematical tool to interpolate multidimensional data [7]: this set of scalar function allow to interpolate data in every point of the definition space using known values at specific points, also called source points. A generic interpolation function can be written as:

$$s(\boldsymbol{x}) = \sum_{i=1}^{N} \gamma_i \varphi \left(\| \boldsymbol{x} - \boldsymbol{x}_{k_i} \| \right) + h(\boldsymbol{x}) \tag{1}$$

In Eq. (1) $\boldsymbol{x}_{k_i}$ are the source points defined in the space $\mathbb{R}^n$ and $\boldsymbol{x}$ are the points at which the function is evaluated, called also target points. φ is the radial function, which is a scalar function of the Euclidean distance between

each source point and the target point considered; most used radial functions are reported in Table 1 , in which $r = (\|\boldsymbol{x} - \boldsymbol{x}_{k_i}\|)$. γ_i are the weights of the radial basis which are to be evaluated solving a linear system of equations, whose order is equal to the number of source points introduced. The polynomial part h is added to guarantee the existence and the uniqueness of the solution. In mesh morphing applications, a linear polynomial can be used:

$$h(\boldsymbol{x}) = \beta_1 + \beta_2 x + \beta_3 y + \beta_4 z \tag{2}$$

in which β_i coefficients are evaluated together with γ_i weights solving the RBF system (see for reference [21]). Once solved, the RBF coefficients and polynomial weights are used to interpolate each imposed displacement component as an independent scalar field:

Table 1. Most common radial functions.

RBF type	Equation
Spline type (Rn)	$r^n,\ n\ odd$
Thin plate spline	$r^n log(r),\ n\ even$
Multiquadric (MQ)	$\sqrt{1+r^2}$
Inverse multiquadric (IMQ)	$\frac{1}{\sqrt{1+r^2}}$
Inverse quadric (IQ)	$\frac{1}{1+r^2}$
Gaussian (GS)	e^{-r^2}

$$\begin{cases} s_x(\boldsymbol{x}) = \sum_{i=0}^{N} \gamma_i^x \varphi\left(\|\boldsymbol{x} - \boldsymbol{x}_i\|\right) + \beta_1^x + \beta_2^x x + \beta_3^x y + \beta_4^x z \\ s_y(\boldsymbol{x}) = \sum_{i=0}^{N} \gamma_i^y \varphi(\|\boldsymbol{x} - \boldsymbol{x}_i\|) + \beta_1^y + \beta_2^y x + \beta_3^y y + \beta_4^y z \\ s_z(\boldsymbol{x}) = \sum_{i=0}^{N} \gamma_i^z \varphi(\|\boldsymbol{x} - \boldsymbol{x}_i\|) + \beta_1^z + \beta_2^z x + \beta_3^z y + \beta_4^z z \end{cases} \tag{3}$$

In mesh morphing, source points are the mesh nodes on which the displacement is imposed, whilst the target nodes are the whole set of nodes that have to be morphed in order to obtain the new numerical model shape.

2.2 Biological Growth Method

BGM allows to perform optimization using as driving quantity surface stress of the considered component. It moves from biological tissues observation: they evolve at surfaces by adding layers when an activation stress is reached.

In [13] and in [17] an extension of this natural mechanism is introduced: as material is added to surfaces where high stresses are present, so material can be removed if acting stresses are low. [13] demonstrated that using photo-elastic techniques and BGM, stresses level can be modified so that uniform stress acts on the boundary of a stress raiser. In [17] a bi-dimensional study that can reproduce the natural evolution of biological structures is illustrated and suggested to be used in optimization workflows: the authors computed the volumetric growth ($\dot{\varepsilon}$) according to the von Mises stress (σ_{Mises}) and a threshold stress (σ_{ref}). The latter one was chosen according to the allowable stress for the specific design:

$$\dot{\varepsilon} = k\,(\sigma_{Mises} - \sigma_{ref}) \tag{4}$$

Waldman and Heller [24] proposed a more complex model for layer growth, which has been successfully employed in shape optimization of holes in airframe structures. The proposed equation to evaluate the nodal displacement is reported in Eq. (5):

$$d_i^j = \left(\frac{\sigma_i^j - \sigma_i^{th}}{\sigma_i^{th}}\right) \cdot s \cdot c \;,\; \sigma_i^{th} = max(\sigma_i^j) \text{ if } \sigma_i^j > 0 \text{ or } \sigma_i^{th} = min(\sigma_i^j) \text{ if } \sigma_i^j < 0 \tag{5}$$

The model by Waldman and Heller moves the i-th boundary node of the j-th region by a distance d_i^j, computed using (5), where σ_i^j is the normal stress in the tangential direction, σ_i^{th} is the stress threshold; c is and arbitrary characteristic length and s is a scaling factor.

In the present work another formulation for BGM is used and implemented in the framework of ANSYS Mechanical, whose functionalities were enhanced by the RBF Morph ACT Extension. RBF Morph BGM approach implementation has been presented in [4]. To each target node (i.e. the set of nodes to be moved in order to perform optimization) a displacement (S_{node}) is imposed along the surface normal direction (inward or outward); the displacement value is calculated using Eq. (6), in which σ_{node} is the stress value for each node, σ_{th} is a threshold value for stress chosen by user, σ_{max} and σ_{min} are the maximum and minimum value for stress evaluated in the current set of source nodes. d is the maximum offset between the nodes on which the maximum and the minimum stress are evaluated. This parameter is defined by the user to control the nodes displacement whilst limiting the possible distortion of the mesh:

$$S_{node} = \frac{\sigma_{node} - \sigma_{th}}{\sigma_{max} - \sigma_{min}} \cdot d \tag{6}$$

Equation (6) allows to impose a displacement for nodes on the surface to be optimized that can be either inward, in case the stress for the current target node is lower than the stress chosen by user as threshold, or outward, in case stress on target node is higher than threshold one.

2.3 Parameter-Less Based Optimisation

The RBF based mesh morphing technique described in Sect. 2.1 and the BGM described in Sect. 2.2 can be coupled so that an automatic optimization approach can be defined, according to the following steps:

1. from the baseline geometry CAD description a finite element model is generated, by discretizing the geometry and setting up the numerical model by adding load and constraints; the FEM solution is then evaluated;
2. BGM routines retrieve nodal stress for target nodes on the model surface to be sculpted, user set both σ_{th} and d parameters of Eq. (6) and S_{node} displacement value for each target node is evaluated;
3. the RBF problem is set up by using the BGM evaluated displacements as values to be interpolated (i.e. surface nodes are used as source nodes). User can complete or improve RBF problem set up by adding more source points (e.g. imposing zero displacement value for those nodes of the model to be maintained fixed);
4. mesh morphing is applied to the FEM model and numerical solution is re-evaluated;
5. new evaluated stress on target nodes are analyzed: if further optimization can be performed the procedure can be repeated starting from point 2; if no additional optimzation steps can be performed, an optimized configuration is reached.

In the proposed workflow, user has to define only two parameters: the stress threshold σ_{th} and the maximum displacement d. The first can be described as the stress value on which the algorithm will try to uniform stress levels on the target nodes; the second parameter is the amount of offset between source nodes in each optimization step: the smaller the value the higher will be the number of steps needed to optimize stress levels and the lower will be the risk of generating distorted mesh which cannot be analyzed by FEM solver.

2.4 Parameter-Based Shape Optimisation

The parameter-based optimization can be performed with RBF mesh morphing by prescribing actions to specific groups of nodes (scaling, translation, surface offset, ...) so that the shape of surfaces and of the volume mesh is updated accordingly. The entity of such actions (scaling factors, component of translation, amount of offset ...) are then combined and controlled so that a certain number of new shapes is generated by Design of Experiment (DoE) and optimal performances are then computed on the response surface [19].

3 Coiled Springs Background

Helical springs are key components of many mechanical systems and have been long studied for decades. Stress distribution on helical springs is not uniform and

both academics and industry researchers are focused on the optimization of wire cross-section by means of stress equalization along cross-section boundary. Thus, many shapes have been proposed to reduce mass or to extend safety and fatigue life of the component. As a matter of fact, most of the engine valve springs have non circular, "ovate" sections. Such optimal shape is obtained as a result of *ad-hoc* numerical optimization algorithms where the stresses are computed using numerical methods like finite or boundary elements. Examples of shape optimisation are given in [14,15].

Optimum spring design would require to meet specifications in terms of stiffness, maximum load, design stress and some geometrical constraints, like solid height and outer and inner radius. As a first step, it is investigated the possibility to use BGM to equalize stresses at cross-section boundaries of a baseline coil, with two different constraints:

1. outer radius is fixed, inside surface is sculpted
2. inner radius is fixed, outside surface is sculpted

The optimized geometries are then compared to equivalent circular cross-section of same stiffness and outer/inner radius. A further comparison is made with a circular cross-section with same stiffness and swept volume, i.e. with same amount of material (and thus weight).

3.1 Equivalent Circular Section

Since the coil is flat and the spring index is moderately large (>6), it is possible to apply basic spring design formulas, as found in [23]. The stiffness of a single coil is:

$$K = \frac{Gd^4}{8D^3} \tag{7}$$

where d is the cross-section diameter, D is mean coil diameter and G is the shear modulus. Due to curvature effect and direct shear, the maximum tangential stress occurs at the inner radius:

$$\tau_{in} = \frac{8PD}{\pi d^3}\left(\frac{4c-1}{4c-4} + \frac{0.615}{c}\right) \tag{8}$$

on the contrary, the minimum stress along the boundary occurs at the outer radius:

$$\tau_{out} = \frac{8PD}{\pi d^3}\left(\frac{4c+1}{4c+4} - \frac{0.615}{c}\right) \tag{9}$$

The design must satisfy the prescribed stiffness and, depending on the case, outer or inner radius.

Constraint on Outer Diameter. For this scenario the spring design must satisfy the following conditions:

$$D + d = D_e \qquad \text{and} \qquad \frac{Gd^4}{8D^3} = K \tag{10}$$

Combining the constraint equations together it is found that the cross-section diameter must satisfy:

$$Gd^4 - 8(D_e - d)^3 K^* = 0 \tag{11}$$

Constraint on Internal Diameter. When the internal diameter is kept constant the geometric constraint writes:

$$D - d = D_i \tag{12}$$

leading to:

$$Gd^4 - 8(D_i + d)^3 K^* = 0 \tag{13}$$

Solving equations gives the diameter of the equivalent wire for prescribed stiffness and geometric constraint.

Constraint on Spring Volume. For a given volume and stiffness coil and wire diameters are given as:

$$D = \left(\frac{2GV^2}{\pi^4 K}\right)^{\frac{1}{5}} \tag{14}$$

$$d = \sqrt{\frac{4\,V}{\pi^2 D}} \tag{15}$$

3.2 Numerical Model of the Coiled Spring

The numerical model represented half coiled spring: it has been modelled in ANSYS Workbench Framework, modelling a 4 mm diameter wire with 20 mm coil radius. At both ends of the coil, cross section area has been increased and connected to the central part of the coil with fillets (see Fig. 1a), in order to mitigate constraints and load application induced stress concentration, ensuring that at the internal section of the modeled wire those effects are not influencing evaluated stress levels. The model was discretized into 74200 parabolic solid

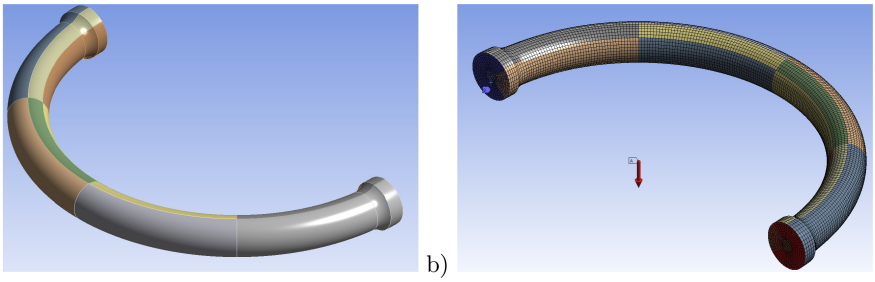

Fig. 1. a) geometry of the modeled half coil, b) load and constraints applied.

elements, resulting in 306569 mesh nodes. A $5N$ external load was applied aligned with the coil axis and connected using ANSYS Mechanical 'Remote Force' load option to mesh nodes on one coil end, whilst the nodes on the other coil end were constrained fixing all degrees of freedom (Fig. 1b).

The BGM based optimization on the half coil geometry was performed according the two optimization constraints described in Sect. 3. In the first one, nodes on the outer coil surface have been fixed and nodes on the inner coil surface have been sculpted (Fig. 2a); in the second one, nodes on the outer coil surface have been sculpted and nodes on the inner coil surface have been constrained (Fig. 2b). For both optimization, the parameters d and S_{node} (Eq. (6)) have been set as 1.2% of the wire diameter and the 80% of the maximum initial stress for Equivalent von Mises Stress acting on coil surfaces. For each optimization, 20 BGM driven mesh morphing iterations were performed.

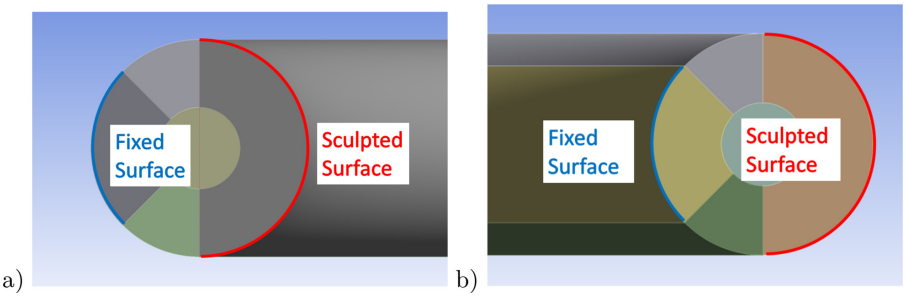

Fig. 2. RBF set up for sculpted coil surfaces (section view): a) inner ones, b) outer ones.

A parameter-based optimization was performed only modifying the inner coil surface, by selecting two groups of nodes (Fig. 3): the first one at the inner point of the coil surface (point 1 in Fig. 3) and the second one placed at 45° in the coil cross section with respect to the inner point location (points 2 in Fig. 3). Both nodes groups were imposed to move along the coil surface normal. The optimization was performed exploiting the ANSYS Desing Explorer optimization tool. The design space was defined setting the displacement range for both nodes groups between 0 and 0.2 mm; the Design of Experiment (DoE) was created according to the Latin Hypercube Sampling Design approach; the DoE results were then used to generate a Kriging response surface with variable kernel. The response surface was then used to identify a parameter configuration which results in coil stress minimization.

4 Results

For both configurations, fixed outer and fixed inner radius, the stiffness has been derived from parameter-less resulting models model and equivalent cross-sections have been calculated using Eqs. (11) and (13); same weight coils have

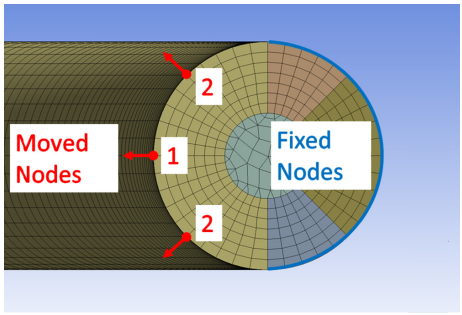

Fig. 3. RBF set up for the parameter-based optimization (section view).

been computed using Eqs. (14) and (15); for the case of fixed outer radius a parameter-based solution was computed as a reference. Optimised shapes are "quasi-elliptical" and can be described in terms of mean diameter D and vertical and horizontal axis of, d_z and d_r respectively.

4.1 Sculpting Inner Surface

When sculpting at the inner radius, the BGM surface sculpting approach moves nodes outward the coil surface, adding material. Optimized section has 3.73% lower maximum stress and 0.6% larger volume with respect to the equivalent circular cross-section. Initial, optimised and equivalent cross-sections are shown in Fig. 4a, stress levels distribution is depicted in Fig. 5a and relevant parameters are listed in Table 2. It can be seen that optimised shape has higher efficiency (41%) than the equivalent circular cross-section (38%), since BGM optimization procedure is adding material where it is more needed. Spring efficiency ϵ is defined as the ratio between the elastic energy stored over the energy the spring would store if all the volume was at maximum stress. Straight torsion bar has 0.5 efficiency, in this case the circular section efficiency is lower because of curvature and direct shear effect. Maximum stress on same weight spring is 4% higher than that on the optimized shape, showing that the optimization is not only improving efficiency but it is also reducing maximum stress.

Table 2. Results for inner surface sculpting - $K = 4.27\,10^4\,[\frac{N}{m}]$

	d_r	d_z	D	τ_{in}/P	τ_{out}/P	ϵ	A	V
	[mm]	[mm]	[mm]	[MPa/N]	[MPa/N]	[–]	mm^2	mm^3
Optimized	4.26	3.85	39.74	1.635	1.273	41%	13.13	1643
Equivalent	4.10	4.10	39.90	1.696	1.280	38%	13.19	1653
Same weight	4.09	4.09	39.80	1.702	1.515	38%	13.14	1643

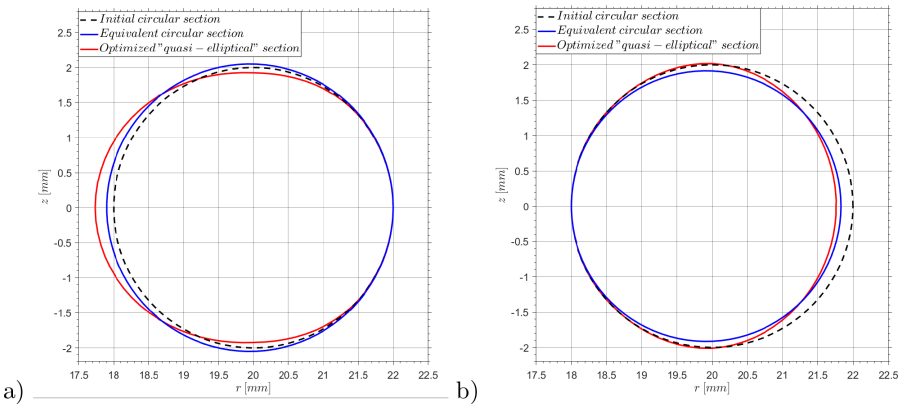

Fig. 4. Cross sections comparison for: a) inner surface sculpting optimization, b) outer surface sculpting optimization.

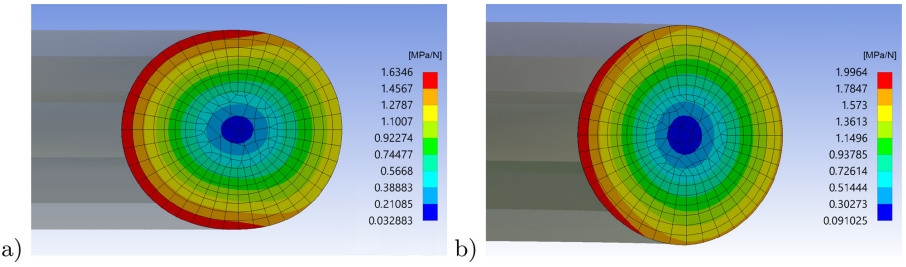

Fig. 5. Stress distribution in section optimized: a) sculpting inner surface, b) sculpting outer surface.

4.2 Sculpting Outer Surface

When sculpting at the outer radius, the BGM moves nodes inward the coils surface, removing material, and reducing maximum stress by 3% and increasing cross-section swept volume by 2.3%, with respect to the equivalent circular cross-section. Baseline, optimised and equivalent circular cross-sections are shown in Fig. 4b, stress levels distribution is depicted in Fig. 5b and relevant parameters are listed in Table 3. It can be seen that in this case the optimisation is not improving the efficiency and is only slightly reducing the maximum stress when compared to an equivalent circular section. More important, the optimized spring performs worse than the same weight spring. In this case the optimization is neither improving the efficiency, nor reducing the maximum stress.

4.3 Optimization Method Comparison

In order to complete the proposed method presentation, a final comparison with the parameter-based response surface optimization method is given. The comparison has been performed with the optimized shape obtained sculpting inner

Table 3. Results for outer surface sculpting - $K = 3.44\,10^4\,[\frac{N}{m}]$

	d_r	d_z	D	τ_{in}/P	τ_{out}/P	ϵ	A	V
	[mm]	[mm]	[mm]	[MPa/N]	[MPa/N]	[–]	[mm^2]	[mm^3]
Optimized	3.76	4.02	39.76	1.996	1.598	38%	11.78	1476
Equivalent	3.83	3.83	39.83	2.055	1.579	38%	11.53	1443
Same weight	3.88	3.88	39.81	1.986	1.777	38%	11.80	1476

surface (see Sect. 4.1 and Fig. 4a). Results for both optimization methods are comparable in terms of maximum surface stress (see Fig. 6a and Fig. 6b). On the other hand, the cross-section area in this configuration is 1.75% higher than the cross-section obtained with the BGM method. The final spring also has a higher stiffness (+3.76%) with respect to the section obtained with the parameters-less optimization and 38% efficiency value, demonstrating how the full reshaping freedom of the parameter-less approach allows to gain slight better results if compared with a 2 parameters optimisation result.

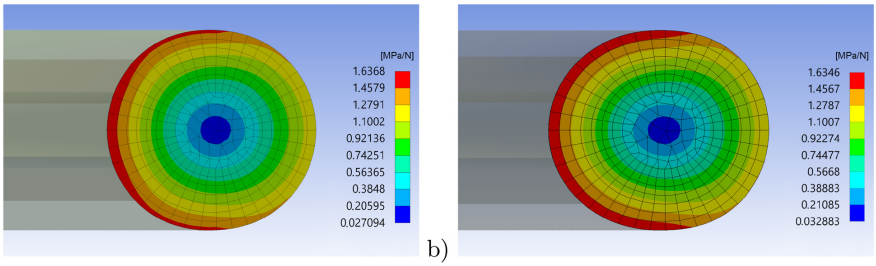

Fig. 6. Stress distribution in section optimized: a) sculpting inner surface with parameter-based method, b) sculpting inner surface with parameter-less method (BGM).

5 Conclusions

In the present work an innovative optimization procedure has been presented. This procedure has been realised by combining an RBF based mesh morphing procedure and a stress level optimization approach based on the observation of natural structures stress mitigation strategies. The reliability of the approach has proven in both implementing in an automatic surface sculpting optimization strategy and in obtaining optimized component shapes.

The focus of the present work was pointed to the optimization of a widely investigated mechanical component, in order to compare the methodology results with the well known and established analytical description of the component itself.

Two optimization constraint were imposed in two optimization tasks: in the first the BGM driven surface sculpting was applied to the inner surface of the coil constraining the outer surface, in the second optimization task the sculpting was applied to the outer surface and the constraint was applied to the inner surface. The first optimization set up gave a final optimized shape that performs better than the circular cross-section, since the BGM driven surface sculpting acts only in adding material on inner surface, where stresses are higher. On the other hand, the optimization through the sculpting of the outer surface failed in improving the design of the component, since BGM is removing material not subject to lowest stress (material should be removed at the core of the cross-section), neither adding it where stress is maximum (i.e. at the inner surface).

Finally, the best results obtained, that are produced by sculpting the inner surface, are compared with the ones computed by a parameter-based optimization of the same region. The obtained shape has comparable performances with respect to the one optimized with the BGM method, but the section efficiency is lower. Furthermore, the parameter-based optimization required more user efforts in setting up of the required DoE and Response Surface model needed to minimize the coil surface stress.

Considering these results, it is possible to say that the proposed automatic surface sculpting optimization approach gave successful results in optimizing the surface coil stress levels.

Acknowledgements. The work here presented is developed within the research project "SMART MAINTENANCE OF INDUSTRIAL PLANTS AND CIVIL STRUCTURES BY 4.0 MONITORING TECHNOLOGIES AND PROGNOSTIC APPROACHES - MAC4PRO", sponsored by the call BRIC-2018 of the National Institute for Insurance against Accidents at Work - INAIL.

References

1. ANSYS, Inc. http://www.ansys.com/products/structures. Accessed 29 July 2020
2. RBF Morph srl. http://www.rbf-morph.com/act-module/. Accessed 29 July 2020
3. Biancolini, M.E.: Mesh morphing and smoothing by means of radial basis functions (RBF): a practical example using Fluent and RBF Morph. In: Handbook of Research on Computational Science and Engineering: Theory and Practice, pp. 347–380. IGI Global (2011)
4. Biancolini, M.E.: Fast Radial Basis Functions for Engineering Applications. Springer, Cham (2017). https://doi.org/10.1007/978-3-319-75011-8
5. Biancolini, M.E., Cella, U.: An advanced RBF morph application: coupled CFD CSM aeroelastic analysis of a full aircraft model and comparison to experimental data. In: MIRA International Vehicle Aerodynamics Conference, Grove, pp. 243–258 (2010)
6. Biancolini, M.E., Chiappa, A., Giorgetti, F., Porziani, S., Rochette, M.: Radial basis functions mesh morphing for the analysis of cracks propagation. Procedia Struct. Integrity **8**, 433–443 (2018)
7. Davis, P.J.: Interpolation and Approximation. Blaisdell Publishing Company, New York (1963)

8. De Boer, A., Van der Schoot, M., Bijl, H.: Mesh deformation based on radial basis function interpolation. Comput. Struct. **85**(11–14), 784–795 (2007)
9. Galland, F., Gravouil, A., Malvesin, E., Rochette, M.: A global model reduction approach for 3D fatigue crack growth with confined plasticity. Comput. Methods Appl. Mech. Eng. **200**(5–8), 699–716 (2011)
10. Giorgetti, F., et al.: Crack propagation analysis of near-surface defects with radial basis functions mesh morphing. Procedia Struct. Integrity **12**, 471–478 (2018)
11. Groth, C., Chiappa, A., Biancolini, M.E.: Shape optimization using structural adjoint and RBF mesh morphing. Procedia Struct. Integrity **8**, 379–389 (2018)
12. Groth, C., Cella, U., Costa, E., Biancolini, M.E.: Fast high fidelity CFD/CSM fluid structure interaction using RBF mesh morphing and modal superposition method. In: Aircraft Engineering and Aerospace Technology (2019). https://doi.org/10.1108/AEAT-09-2018-0246
13. Heywood, R.B.: Photoelasticity for Designers. Pergamon Press, Oxford (1969)
14. Imaizumi, T., Ohkouchi, T., Ichikawa, S.: Shape optimization of the wire cross section of helical springs. SAE Tech. Paper **920775**, 775 (1990)
15. Kamiya, N., Kita, E.: Boundary element method for quasi-harmonic differential equation with application to stress analysis and shape optimization of helical spring. Comput. Struct. **37**(1), 81–86 (1990). https://www.sciencedirect.com/science/article/pii/004579499090199C
16. Lombardi, M., Parolini, N., Quarteroni, A.: Radial basis functions for inter-grid interpolation and mesh motion in FSI problems. Comput. Methods Appl. Mech. Eng. **256**, 117 (2013)
17. Mattheck, C., Burkhardt, S.: A new method of structural shape optimization based on biological growth. Int. J. Fatigue **12**(3), 185–190 (1990)
18. Papoutsis-Kiachagias, E.M., Porziani, S., Groth, C., Biancolini, M.E., Costa, E., Giannakoglou, K.C.: Aerodynamic optimization of car shapes using the continuous adjoint method and an RBF morpher. In: Minisci, E., Vasile, M., Periaux, J., Gauger, N.R., Giannakoglou, K.C., Quagliarella, D. (eds.) Advances in Evolutionary and Deterministic Methods for Design, Optimization and Control in Engineering and Sciences. CMAS, vol. 48, pp. 173–187. Springer, Cham (2019). https://doi.org/10.1007/978-3-319-89988-6_11
19. Porziani, S., Groth, C., Biancolini, M.E.: Automatic shape optimization of structural components with manufacturing constraints. Procedia Struct. Integrity **12**, 416–428 (2018)
20. Porziani, S., Groth, C., Mancini, L., Cenni, R., Cova, M., Biancolini, M.E.: Optimisation of industrial parts by mesh morphing enabled automatic shape sculpting. Procedia Struct. Integrity **24**, 724–737 (2019)
21. Porziani, S., Groth, C., Waldman, W., Biancolini, M.E.: Automatic shape optimisation of structural parts driven by BGM and RBF mesh morphing. Int. J. Mech. Sci. 105976 (2020). http://www.sciencedirect.com/science/article/pii/S0020740320306184
22. Staten, M.L., Owen, S.J., Shontz, S.M., Salinger, A.G., Coffey, T.S.: A comparison of mesh morphing methods for 3D shape optimization. In: Proceedings of the 20th International Meshing Roundtable, pp. 293–311. Springer, Cham (2011). https://doi.org/10.1007/978-3-642-24734-7_16
23. Wahl, A.M.: Mechanical Springs. McGraw-Hill Book Company Inc., New York (1963)
24. Waldman, W., Heller, M.: Shape optimisation of holes in loaded plates by minimisation of multiple stress peaks. Technical Report DSTO-RR-0412, Aerospace Division, Defence Science And Technology Organisation, Melbourne (2015)